

Provided for non-commercial research and education use.
Not for reproduction, distribution or commercial use.



This article appeared in a journal published by Elsevier. The attached copy is furnished to the author for internal non-commercial research and education use, including for instruction at the authors institution and sharing with colleagues.

Other uses, including reproduction and distribution, or selling or licensing copies, or posting to personal, institutional or third party websites are prohibited.

In most cases authors are permitted to post their version of the article (e.g. in Word or Tex form) to their personal website or institutional repository. Authors requiring further information regarding Elsevier's archiving and manuscript policies are encouraged to visit:

<http://www.elsevier.com/copyright>



Contents lists available at SciVerse ScienceDirect

International Journal of Heat and Mass Transfer

journal homepage: www.elsevier.com/locate/ijhmt

Convective heat transfer in foams under laminar flow in pipes and tube bundles

Joseph A. Attia, Ian M. McKinley, David Moreno-Magana, Laurent Pilon*

Mechanical and Aerospace Engineering Department, University of California, Los Angeles, Los Angeles, CA 90095, USA

ARTICLE INFO

Article history:

Received 8 March 2012

Received in revised form 2 August 2012

Accepted 4 August 2012

Available online 18 September 2012

Keywords:

Non-Newtonian fluids

Foams

Pseudoplastic fluids

Shear thinning fluids

Power law fluids

Two-phase flow heat transfer

Colloidal gas aphanons

ABSTRACT

The present study reports experimental data and scaling analysis for forced convection of foams and microfoams in laminar flow in circular and rectangular tubes as well as in tube bundles. Foams and microfoams are pseudoplastic (shear thinning) two-phase fluids consisting of tightly packed bubbles with diameters ranging from tens of microns to a few millimeters. They have found applications in separation processes, soil remediation, oil recovery, water treatment, food processes, as well as in fire fighting and in heat exchangers. First, aqueous solutions of surfactant Tween 20 with different concentrations were used to generate microfoams with various porosity, bubble size distribution, and rheological behavior. These different microfoams were flowed in uniformly heated circular tubes of different diameter instrumented with thermocouples. A wide range of heat fluxes and flow rates were explored. Experimental data were compared with analytical and semi-empirical expressions derived and validated for single-phase power-law fluids. These correlations were extended to two-phase foams by defining the Reynolds number based on the effective viscosity and density of microfoams. However, the local Nusselt and Prandtl numbers were defined based on the specific heat and thermal conductivity of water. Indeed, the heated wall was continuously in contact with a film of water controlling convective heat transfer to the microfoams. Overall, good agreement between experimental results and model predictions was obtained for all experimental conditions considered. Finally, the same approach was shown to be also valid for experimental data reported in the literature for laminar forced convection of microfoams in rectangular minichannels and of macrofoams across aligned and staggered tube bundles with constant wall heat flux.

© 2012 Elsevier Ltd. All rights reserved.

1. Introduction

Microfoams consist of tightly packed spherical bubbles between 10 and 100 μm in diameter with a porosity of up to 70% [1]. They can be produced by spinning a disk at 5000–10,000 rpm in an aqueous surfactant solution contained in a baffled beaker at room temperature [1]. Such microfoams have also been termed colloidal gas aphanons (CGA) [1]. However, the multiple surfactant-shell structure forming around individual bubbles proposed by Sebba [1] has not been directly and unequivocally observed [2]. Thus, we prefer to call this two-phase fluid “microfoams” instead of “CGA”. Microfoams have found numerous applications including separation processes [3–5], soil remediation [5–7], water treatment [8,9], and biotechnology [10]. These applications take advantage of (i) their large interfacial area, (ii) the adsorption of particles at the microbubble interfaces, and (iii) their stability for enhanced mass transfer [11]. Microfoam made from mixtures of anionic and cationic surfactants have also been shown to spread over a pool of burning gasoline and to extinguish fire [1].

Moreover, traditional macrofoams are commonly used as fire suppressant [12]. They have also been used as a fracturing fluid

for improved oil recovery. Then, convective heat transfer takes place between the rock formation and the foams [13]. Finally, macrofoams have also been considered as a working fluid in heat exchangers to take advantage of the fact that the associated heat transfer coefficient is significantly larger than that achieved using air under the same conditions [14,15]. This could reduce the size and mass of air-based heat exchangers.

In these various applications, it is important to understand and predict transport phenomena in foams including convective heat transfer. The present study investigates experimentally forced convection in microfoams flowing in circular tubes under laminar flow conditions and subject to constant wall heat flux. It also presents a scaling analysis for convective heat transfer in microfoams in rectangular minichannels and macrofoams in tube bundles under laminar flow.

2. Background

2.1. Microfoam rheology

The rheological behavior of foams and microfoams can be described by the pseudoplastic power-law model expressed as [16],

$$\tau_w = K_p \dot{\gamma}_w^n = K_p' \dot{\gamma}_a^n = \mu_f \dot{\gamma}_a \quad (1)$$

* Corresponding author. Tel.: +1 310 206 5598; fax: +1 310 206 4830.

E-mail address: pilon@seas.ucla.edu (L. Pilon).

Nomenclature

A	cross-sectional area of test section (m ²)	$T_i(x_i)$	inner wall temperature at location x_i (K)
Ca^*	volume equalized capillary number, Eq. (3)	$T_{wall}(x_i)$	outer wall temperature at location x_i (K)
$C(\chi)$	empirical function, Eq. (4)	t	time (s)
c_p	specific heat (J/kg K)	U_{max}	maximum velocity in minimum flow area (m/s)
D_h	hydraulic diameter (m)	ϑ	voltage (V)
h_x	local heat transfer coefficient (W/m ² K)	V_f	volume of microfoams (mL)
I	current (A)	V_p	volume of tube bundles (m ³)
k	thermal conductivity (W/m K)	x	dimensional axial length (m)
K_p	flow consistency constant	x_i	thermocouple location from pipe entrance (m)
L	length of the test section (m)	x^*	dimensionless axial length for cylindrical pipe, $x^* = 2x/D_h Re_D Pr$
l_L	dimensionless longitudinal pitch, Eq. (15)		
l_T	dimensionless traverse pitch, Eq. (15)		
\dot{m}	mass flow rate (kg/s)	Greek symbols	
M_f	mass of microfoam (Kg)	α	rectangular channel aspect ratio, (α = width/height)
n	flow behavior index	χ	surfactant mass fraction (wt.%)
Nu_x	local Nusselt number, $Nu_x = h_x D_h / k$	ϵ	specific expansion ratio
$Nu_{D,exp}$	experimental local Nusselt number for tube bundles, Eq. (27)	ϕ	microfoam porosity
Nu_∞	Nusselt number for thermally fully developed conditions	$\dot{\gamma}_a$	apparent shear rate (1/s)
Pr	Prandtl number, $Pr = c_p \mu / k$	$\dot{\gamma}_w$	wall shear rate (1/s)
\dot{Q}	volumetric flow rate (m ³ /s)	μ	dynamic fluid viscosity (Pa s)
q_f	actual heat input to the microfoam (W)	σ	surface tension (N/m)
q_{loss}	heat loss to the surrounding (W)	τ_w	wall shear stress (Pa)
q_{total}	total power input (W)	τ^*	dimensionless shear stress
q_w''	wall heat flux (W/m ²)		
Re_D	Reynolds number, $Re = \rho \dot{Q} / \frac{1}{4} \pi D_h \mu$	Subscripts	
$Re_{D,max}$	Reynolds number for flows across tube bundles, Eq. (13)	f	refers to microfoam or foam property
r_i	inner pipe radius (m)	g	refers to air in microfoam
r_o	outer pipe radius (m)	$pipe$	refers to stainless steel pipe property
r_{32}	Sauter mean bubble radius (m)	w	refers to water property or wall shear
$T_f(x_i)$	average local temperature of microfoams (K)	3,4	refers to rectangular channels heated from 3 or 4 walls
T_{in}	microfoam temperature at test section inlet (K)		
T_{out}	microfoam temperature at test section outlet (K)	Superscript	
		*	refers to power-law fluid dimensionless numbers and correlations

where τ_w is the wall shear stress, $\dot{\gamma}_w$ is the true wall shear rate, and $\dot{\gamma}_a$ is the apparent shear rate while the effective foam viscosity is denoted by μ_f . The empirical constants K_p and n are the so-called flow consistency and flow behavior index, respectively. The true wall shear rate $\dot{\gamma}_w$ can be derived from $\dot{\gamma}_a$ through the Rabinowitsch–Mooney relationship [17],

$$\dot{\gamma}_w = \left(\frac{3n+1}{4n}\right)\dot{\gamma}_a \quad \text{and} \quad K'_p = K_p \left(\frac{3n+1}{4n}\right)^n \quad (2)$$

Recently, Larmignat et al. [16] investigated the rheology of microfoams flowing through cylindrical pipes. Experimental data were collected for aqueous solutions of non-ionic surfactant polyoxyethylene (20) sorbitan monolaurate (Tween 20) with mass fraction ranging from 0.03 to 9.96 wt.%. The authors defined the volume equalized dimensionless shear stress and Capillary number as

$$\tau^* = \frac{\tau_w r_{32}}{\sigma \epsilon} \quad \text{and} \quad Ca^* = \frac{\mu_w r_{32} \dot{\gamma}_a}{\epsilon \sigma} \quad (3)$$

where r_{32} is the Sauter mean bubble radius, σ is the surface tension, μ_w is the viscosity of water, and ϵ is the specific expansion ratio defined as the ratio of the densities of the liquid phase and microfoam. Experimental data established that $\tau^* = C(\chi)(Ca^*)^{2/3}$ where $C(\chi)$ is an empirical function dependent on the surfactant mass fraction χ (in wt.%). In practice, microfoams made with aqueous solutions of Tween 20 can be treated as a shear-thinning fluid with an effective viscosity given by [16],

$$\mu_f = \mu_w C(\chi)(Ca^*)^{-1/3} \quad \text{with} \quad C(\chi) = 0.4 + 0.8(1 - e^{-\chi/0.018}) \quad (4)$$

These results were in good agreement with the model developed by Denkov et al. [18,19] for foams with porosity larger than 90% made of fluids with low surface dilatational modulus resulting typically in tangentially mobile bubble surface. They were also confirmed by experimental measurements for anionic and cationic surfactants including hexadecyl–trimethyl–ammonium bromide (CTAB) and sodium lauryl sulfate (SDS) [20].

2.2. Convective heat transfer in power-law fluids in circular pipes

Bird [21] derived an analytical solution predicting the local Nusselt number in the entry region Nu_x^* and in the thermally fully developed region Nu_∞^* for single phase power-law fluids with flow behavior index n flowing through circular pipes subject to constant wall heat flux as,

$$Nu_x^* = \frac{h_x D_h}{k} = 1.41 \left(\frac{3n+1}{4n}\right)^{1/3} \left(\frac{2}{x^*}\right)^{1/3} \quad \text{and} \quad Nu_\infty^* = \frac{8(5n+1)(3n+1)}{31n^2 + 12n + 1} \quad (5)$$

Here, D_h is the hydraulic diameter of the wetted perimeter, k is the thermal conductivity of the power-law fluid, and h_x is the local heat transfer coefficient. The dimensionless axial length x^* is defined as $x^* = 2x/D_h Re_D Pr$ where x is the axial location measured from the heated pipe entrance. The Reynolds and Prandtl numbers respectively denoted by Re_D and Pr were defined as,

$$Re_D = \frac{4\rho\dot{Q}}{\pi D_h \mu} \quad \text{and} \quad Pr = \frac{c_p \mu}{k} \quad (6)$$

where c_p is the specific heat of the power-law fluid, ρ is the fluid density, μ is the fluid effective dynamic viscosity, and \dot{Q} is the volumetric flow rate.

Alternatively, Joshi and Bergles [22] applied a non-Newtonian correction factor developed by Mizushima et al. [23] to the correlation for Newtonian fluids proposed by Churchill and Usagi [24]. For constant fluid thermal properties this model is expressed as [22],

$$Nu_x^* = 4.36 \left(\frac{3n+1}{4n} \right)^{1/3} \{ 1 + [0.376(x^+)^{-0.33}]^6 \}^{1/6}. \quad (7)$$

The authors experimentally validated this model with a single-phase power-law fluid made from 0.9 and 1.0 wt.% aqueous solution of hydroxy ethyl methyl cellulose (HEMC) flowing through a circular pipe subject to constant wall heat flux. Note that thermally fully developed flow is reached when the dimensionless axial length x^+ is greater than 0.1 [25]. In addition, for flow behavior $n = 2/3$, such as that exhibited by microfoams [16,18–20], the local Nusselt number predicted by Eqs. (5) and (7) falls within 10% of each other in the entry region and within 4% in the fully developed region.

Furthermore, Tseng et al. [26] experimentally investigated both the rheology and convective heat transfer of microfoams made of Tween 20 in horizontal minichannels with a rectangular cross-section and heated from three walls. The authors found that the local heat transfer coefficient and Nusselt number for microfoams under imposed heat flux and laminar flow conditions were independent of mass flow rate and heat flux. These results were similar to observations and theory for Newtonian fluids under the same conditions [27]. They also determined that the heat transfer coefficient for microfoams made of aqueous surfactant solutions was smaller than for single-phase water due to the microfoams' large porosity and low thermal conductivity.

More recently, Gylys et al. [14,15] investigated convective heat transfer in dry aqueous foams with porosity of 99.6%, 99.7% and 99.8% and velocities between 0.14 m/s and 0.32 m/s. The authors reported the local heat transfer coefficient as a function of fluid velocity for upward and downward vertical aqueous foam flow across staggered and aligned tube bundles of diameter $D = 0.02$ m at different tube locations. Foams were generated by injecting gas in an aqueous surfactant solution through a perforated plate with 1 mm holes. Unfortunately, (i) the type of surfactant used to make the foam, (ii) the surface tension of the air/solution system, and (iii) the average bubble radius were not reported. Therefore, it was impossible to estimate the foam's effective viscosity and capillary number. Gylys et al. [14,15] derived an empirical correlations for predicting the local Nusselt number, based on the effective foam thermal conductivity given by the parallel model. The average Nusselt number was expressed as a function of the gas phase Reynolds number for foam flow across staggered tube bundles [14]. The average heat transfer coefficient was given as a function of foam porosity and velocity for foam flow across the aligned tube bundle [15]. Unfortunately, these correlations were derived from a limited data set with specific geometric features and therefore the validity of these correlations for other tube bundle dimensions and different foam properties is unknown.

2.3. Convective heat transfer in rectangular channels

Lee and Garimella [28] derived a generalized correlation for predicting the local Nusselt number $Nu_{x,4}$ for convective heat transfer of laminar Newtonian flow in rectangular microchannels with constant wall heat flux from all four sides. It is expressed as [28]

$$Nu_{x,4} = \frac{h_x D_h}{k} = \frac{1}{C_1 (x^+/2)^{C_2} + C_3} + C_4 \quad (8)$$

where C_1 , C_2 , C_3 , and C_4 are empirical constants depending on the aspect ratio α of the rectangular channel ($1 \leq \alpha \leq 10$) and given by Eq. (12) in Ref. [28]. Secondly, the dimensionless axial length x^+ is defined as previously using Re_D based on the hydraulic diameter of the channel D_h .

For constant wall heat flux from three sides with one adiabatic side, Phillips [29] introduced a correction factor to express the Nusselt number as,

$$Nu_{x,3} = Nu_{x,4} \times \left(\frac{Nu_{\infty,3}}{Nu_{\infty,4}} \right) \quad (9)$$

Here, $Nu_{\infty,3}$ and $Nu_{\infty,4}$ are the fully developed Nusselt number for three and four sided uniform wall heat flux boundary conditions, respectively expressed as [30]

$$Nu_{\infty,3} = 8.235 \left(1 - \frac{1.883}{\alpha} + \frac{3.767}{\alpha^2} - \frac{5.814}{\alpha^3} + \frac{5.361}{\alpha^4} - \frac{2.0}{\alpha^5} \right) \quad (10)$$

and

$$Nu_{\infty,4} = 8.235 \left(1 - \frac{2.0421}{\alpha} + \frac{3.0853}{\alpha^2} - \frac{2.4765}{\alpha^3} + \frac{1.0578}{\alpha^4} - \frac{0.1861}{\alpha^5} \right) \quad (11)$$

2.4. Convective heat transfer in tube bundles

Khan et al. [31,32] presented an analytical correlation for single phase convective heat transfer in laminar flows across aligned and staggered tube bundles under constant temperature and wall heat flux. The average Nusselt number over the entire tube bundle in the fully developed region was expressed as

$$\bar{Nu}_{D,th} = C_5 Re_{D,max}^{1/2} Pr^{-1/3} \quad (12)$$

where C_5 is a constant depending on the tube arrangement while the Reynolds number $Re_{D,max}$ was defined based on the maximum fluid velocity U_{max} as [32]

$$Re_{D,max} = \frac{\rho U_{max} D}{\mu} \quad (13)$$

The maximum velocity in the minimum flow area is denoted by U_{max} and expressed as [32]

$$U_{max} = \max \left(\frac{l_T}{l_T - 1} \dot{Q}_f / A, \frac{l_T}{l_D - 1} \dot{Q}_f / A \right) \quad (14)$$

where A is the cross-sectional area of the test section and $l_D = \sqrt{l_L^2 + (l_T/2)^2}$ while l_T and l_L are the dimensionless longitudinal and transverse pitches defined as [32]

$$l_L = s_L / D \quad \text{and} \quad l_T = s_T / D \quad (15)$$

Here, s_L and s_T are the interaxial distance between tubes of diameter D in the direction of the flow and normal to the flow, respectively.

Finally, the above correlations Eqs. (5) and (7) have been validated and used for single-phase power-law fluids. However, it is not clear whether they are valid for two-phase fluids such as foams and microfoams. To the best of our knowledge, no experimental data and analysis have been reported for forced convective heat transfer in microfoams flowing in cylindrical pipes. The present study aims to collect experimental data for convective heat transfer of microfoams in laminar pipe flow under constant heat flux. It also aims to adapt existing correlations developed for single-phase Newtonian and power-law fluids to two-phase microfoams in rectangular minichannels and macrofoams in tube bundles.

3. Experiments

3.1. Experimental setup

In the present study, microfoams were generated by continuously stirring an aqueous surfactant solution with a Silverson L4RT mixer at 7000 rpm in a baffled container as described in detail in Refs. [16,20]. The aqueous surfactant solutions were made by mixing Tween 20 purchased from USB Corp. (USA) in deionized water with mass fraction χ equal to 0.22, 0.55, 2.17, and 4.23 wt.%. The container was placed in a large tank of water acting as a thermal reservoir to maintain the microfoam at constant temperature. Type-T thermocouples were used to monitor the microfoam and water temperatures. The microfoam was continuously produced and pumped into the test section to ensure that it had the same inlet morphology, porosity, and temperature. The foam porosity, Sauter mean bubble radius, and surface tension of the solution/air system were reported in Table 1 of Ref. [16].

The experimental setup was typical of a pipe flow experiment and consisted of (i) a supply tank, (ii) a volumetric pump (Cole-Parmer, model 75225), (iii) a data acquisition system (IOTECH DAQTEMP 14 A) connected to a personal computer, and (iv) a test section shown in Fig. 1. The test section consisted of a 0.305 m long stainless steel 304 cylindrical pipe tightly fitted through a copper rod. The pipes had inner diameter equal to 1.52 mm or 2.41 mm with corresponding outer diameter equal to 1.78 mm or 3.15 mm. Sealing was achieved by soldering the steel pipe and the copper rods. The latter was then screwed into Teflon rods used to connect the test section with the rest of the experimental setup. A differential pressure sensor (Omega PX26-015DV) was used to measure the pressure drop between the inlet and outlet of the pipe (Fig. 1). The pressure drop was corrected for minor losses due to sudden expansion and contraction in the test section (Fig. 1). Microfoam rheology was discussed in details in Ref. [16] and need not be repeated. The test section was heated by connecting the leads of a Sorensen DCS8-125E power supply to the copper rods thereby flowing a constant current and thus creating a constant wall heat flux along the stainless steel pipe (Fig. 1). The microfoam temperatures at the inlet and outlet of the test section were measured by type-K thermocouples. Likewise, seven type-K thermocouples were mounted axially along the top of the stainless steel pipe's outer wall with high thermal conductivity cement. The seven thermocouple axial locations x_i measured from the channel entrance were $x_1 = 0.027$ m, $x_2 = 0.056$ m, $x_3 = 0.078$ m, $x_4 = 0.118$ m, $x_5 = 0.157$ m, $x_6 = 0.197$ m, and $x_7 = 0.260$ m as illustrated in Fig. 1. The test section was supported by G10 slabs placed above

and underneath the pipe to ensure that it remained straight and horizontal. The heated pipe was also thermally insulated from the surroundings by several centimeters of fiberglass insulation to minimize heat losses.

Finally, the volume of microfoam $V_f(t)$ flowing out of the test section between times 0 and t was determined by using either a graduated Kimax 100 mL cylinder or a Nalgene 1 L beaker while the time t was measured by a stop watch. Simultaneously, the corresponding mass of microfoam $M_f(t)$ was measured by using a compact digital bench Ohaus Scout Pro SP401 scale. The plots of $V_f(t)$ and $M_f(t)$ as functions of time were linear and their slopes were the volumetric flow rate \dot{Q}_f and the mass flow rate \dot{m}_f of microfoam, respectively. The microfoam density ρ_f was experimentally determined by dividing the mass flow rate \dot{m}_f by the volumetric flow rate \dot{Q}_f , i.e., $\rho_f = \dot{m}_f / \dot{Q}_f$. The microfoam porosity, defined as the ratio of the volume of gas to the total volume of foam, was estimated by [26]

$$\phi = 1 - \frac{\dot{m}_f}{\rho_w \dot{Q}_f} = 1 - \frac{\rho_f}{\rho_w} \quad (16)$$

where ρ_w is the density of water.

3.2. Experimental procedure and data reduction

The parameters measured experimentally for different values of flow rate and heat input were (i) the pressure drop along the cylinder, (ii) the inlet and outlet temperatures T_{in} and T_{out} , (iii) the local temperatures along the outer pipe wall $T_{wall}(x_i)$, (iv) the volumetric flow rate \dot{Q}_f , (v) the mass flow rate \dot{m}_f , and (vi) the microfoam density ρ_f and porosity ϕ .

Prior to collecting the data, the microfoam was flowed through the heated pipe for 5–10 min to ensure that a steady state had been reached. Then, the temperature readings were recorded for 1 min and averaged. In addition, micrographs of the microfoam were taken at the inlet and outlet of the test section to verify that the microfoam morphology did not change significantly as it was flowed and heated in the pipe. Note that the residence time of the microfoams in the heated pipe was less than 3 s for the volumetric flow rates considered. Given the short residence time in the connecting pipes and in the test section, flow stratification caused by liquid drainage between the microfoam generation point and exit of the test section was assumed to be negligible.

The total power input was determined as the product of the current I and voltage ϑ applied across the test section,

$$q_{total} = \vartheta I. \quad (17)$$

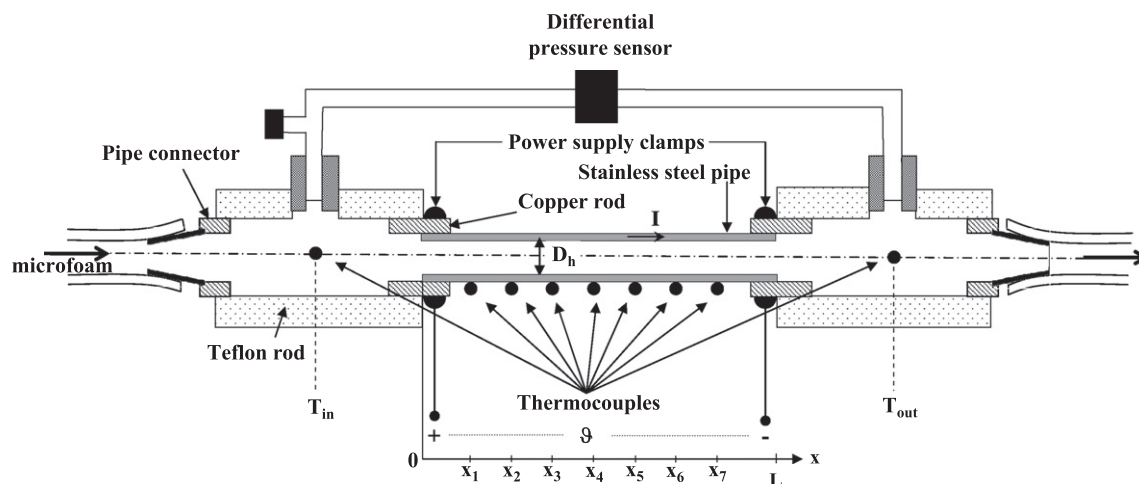


Fig. 1. Schematic of the experimental test section used along with dimensions and locations of the thermocouples.

The actual heat input from the wall to the microfoam q_f was determined from an energy balance on the microfoam given by,

$$q_f = \dot{m}_f c_{p,f} (T_{out} - T_{in}) \quad (18)$$

where $c_{p,f}$ is the specific heat of microfoam at the average temperature expressed as [26]

$$\rho_f c_{p,f} = \rho_w (1 - \phi) c_{p,w} + \rho_g \phi c_{p,g}. \quad (19)$$

Here, ρ_g and $c_{p,g}$ are the density and specific heat of air, respectively, while ρ_w and $c_{p,w}$ are those of water.

The heat losses to the surroundings were quantified by subtracting the total heat input from the actual input into the microfoam, i.e., $q_{loss} = q_{total} - q_f$. In the present study, approximately 90% of the total electric power consumed was transferred to the microfoam flowing in the test section, i.e., heat losses from the test section to the surroundings were about 10%.

Finally, the wall heat flux q''_w was calculated from the heat input q_f to the microfoam according to,

$$q''_w = q_f / \pi D_h L \quad (20)$$

where L is the length of the heated test section.

Furthermore, the cylinder inner wall temperature $T_i(x_i)$ at specified axial locations $(x_i)_{1 \leq i \leq 7}$ were determined from temperature measurements at the outer wall $T_{wall}(x_i)$ by correcting for radial heat conduction through the pipe according to [26]

$$T_i(x_i) = T_{wall}(x_i) + \ln(r_o/r_i) q''_w r_i / k_{pipe} \quad (21)$$

where $k_{pipe} = 14.9 \text{ W/m K}$ [27] is the thermal conductivity of the stainless steel pipe used in the experiment and r_i and r_o are its inner and outer radii, respectively. The local temperature of the microfoam, $T_f(x)$ at different axial locations was estimated based on an energy balance given by [27],

$$T_f(x_i) = T_{in} + \left(\frac{T_{out} - T_{in}}{L} \right) x_i. \quad (22)$$

Then, the local heat transfer coefficient at location x_i was expressed as [26]

$$h_x(x_i) = \frac{q''_w}{T_f(x_i) - T_i(x_i)}. \quad (23)$$

Finally, measurement uncertainties associated with the data were (i) $\pm 5 \text{ mL}$ for volume V_f , (ii) $\pm 1.0 \text{ g}$ for mass M_f , (iii) $\pm 5\%$ for the volumetric flow rate \dot{Q}_f , (iv) $\pm 0.01 \text{ V}$ for the voltage ϑ , (v) $\pm 0.01 \text{ A}$ for the current I , and (vi) $\pm 0.2 \text{ }^\circ\text{C}$ for the temperature measurements T_{in} , T_{out} , and $T_{wall}(x_i)$. All properties were evaluated at the arithmetic mean of the inlet and outlet temperatures.

4. Results and discussion

4.1. Validation

The experimental procedure and data reduction were validated with single-phase deionized water flowing in 2.4 mm diameter pipe under laminar flow conditions with constant wall heat flux. Analytical expressions for the local Nusselt number Nu_x as a function of dimensionless axial length of the pipe $x^+ = 2x/D_h Re_D Pr$ for these conditions were reported in Eq. (8-42) in Ref. [33] and Eq. (6.137) in Ref. [34]. Fig. 2 compares Nu_x versus x^+ predicted by these expressions with our experimental data obtained with deionized water for wall heat transfer rate ranging from 74 to 125 W and Reynolds number between 727 and 1362. The dimensionless numbers were estimated using fluid properties [35] determined at $(T_{in} + T_{out})/2$. It is evident that the local Nusselt number decreased in the entry region as the thermal boundary layer developed. It reached a constant value independent of heat flux

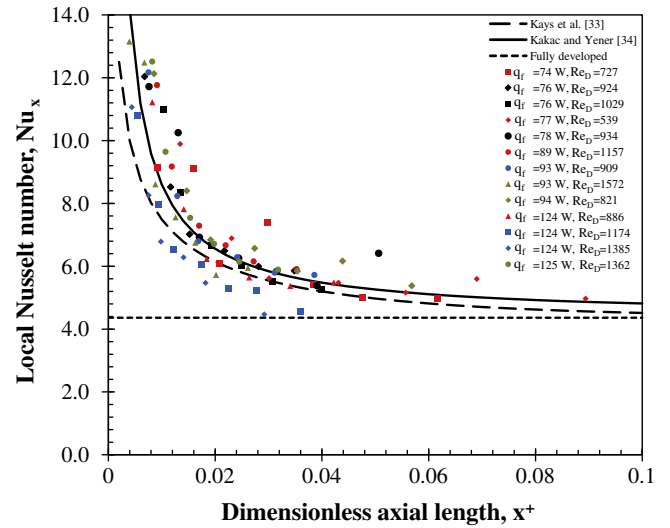


Fig. 2. Comparison of the local Nusselt number as a function of dimensionless axial length of the pipe $x^+ = 2x/D_h Re_D Pr$ between experimental measurements and predictions from correlations given by Eq. (8-42) in Ref. [33] and Eq. (6.137) in Ref. [34] for laminar flow of single-phase deionized water under constant heat flux in 2.4 mm diameter pipe.

and Reynolds number in the thermally fully developed region where $Nu_x = 4.36$ [27]. These results establish the validity of the experimental setup and data analysis.

4.2. Scaling analysis for convective heat transfer in foams

The dimensionless numbers Re_D , Nu_x , and Pr used in correlations for single-phase power-law fluids were given by Eqs. (5) and (6). However, for microfoams it remains unclear what expressions and fluid properties ρ , μ , c_p , and k should be used. One could treat microfoams as a homogeneous fluid with some effective properties estimated using an effective medium approximation (EMA). For example, a wide variety of EMAs exist for estimating the effective thermal conductivity k_f of heterogeneous materials including the series and parallel models [36] as well as Russel [37], son Frey [38], Rayleigh [39], De Vries [40], Maxwell [41], Bruggeman [42], and the dispersion thermal conductivity [43] models. However, no specific model has been validated for the thermal conductivity of microfoams. Note that experimental measurements are made difficult by the foam metastability and relatively rapid decay.

Alternatively, L ev eque's approximation [44], commonly applied to power-law fluids, assumes that at the wall the temperature boundary layer is controlled by a thin layer of fluid. In the case of aqueous foams, the heated wall is in direct and continuous contact with a thin layer of water separating the bubbles from the wall [18,19] and controlling the overall convective heat transfer from the wall to the foam. In addition, based on scaling analysis of the boundary layer equations, the Nusselt number can be interpreted as a dimensionless temperature gradient at the fluid/wall interface [27]. Thus, it is reasonable to define the Nusselt and Prandtl numbers based on the thermal properties of water, namely $c_{p,w}$ and k_w , as opposed to the effective properties of foams. However, from a rheological point of view, microfoams and macrofoams were shown to flow like a single-phase power-law fluid with some effective viscosity and density [16,18,20]. Then, the Reynolds number can be defined based on the effective physical properties of the microfoam, namely ρ_f and μ_f . In summary, for forced convection in foams, we define the dimensionless numbers Nu_x^* , Re_D^* and Pr^* , respectively, as,

$$Re_D^* = \frac{4\rho_f \dot{Q}_f}{\pi D_h \mu_f}, \quad Nu_x^* = \frac{h_x D_h}{k_w}, \quad \text{and} \quad Pr^* = \frac{c_{p,w} \mu_f}{k_w} \quad (24)$$

4.3. Results

The experimental data collected covered a broad range of microfoam properties as well as hydrodynamic and thermal conditions. In fact, the surfactant mass fraction ranged from 0.22 to 4.23 wt.% resulting in microfoams density between 254 kg/m³ and 422 kg/m³ corresponding to a porosity ϕ between 0.58 and 0.74. The microfoam volumetric flow rate \dot{Q}_f varied between 0.336 cm³/s and 1.46 cm³/s. As a consequence, the effective viscosity μ_f of the microfoam varied from 0.005 N s/m² to 0.022 N s/m². Finally, the wall heat flux q_w'' was varied between 4360 W/m² and 21,380 W/m². In all cases (i) the microfoam Reynolds number was less than 1000 so that the flow was laminar and (ii) the dimensionless axial length x^+ reached at least 0.1 to ensure that thermally fully developed conditions were reached by the end of the test section. The uncertainty in the temperature measurements contributed an average of $\pm 7\%$ error to the experimentally determined Nusselt number.

First, Fig. 3 shows the measured heat transfer coefficient h_x estimated using Eq. (23) versus the axial location x for microfoams made of surfactant solution with concentration 2.17% flowing in pipes with diameter 1.5 mm and 2.4 mm under various wall heat fluxes and mass flow rates. It indicates that the heat transfer coefficient decreased along the channel length and approached a constant value for large enough values of x .

Fig. 4 shows the local Nusselt number Nu_x^* versus the dimensionless axial length $x^+ = 2x/D_h Re_D^* Pr^*$ obtained with microfoams for all Tween 20 mass fractions, heat fluxes, and flow rates considered. The dimensionless numbers Nu_x^* , Re_D^* , and Pr^* were defined according to Eq. (24). Fig. 4 indicates that Nu_x^* decreased in the entry region and reached a constant in the fully developed region. The spread in the experimental data can be attributed to differences in porosity, bubble size distribution, and viscosity caused by differences in surfactant concentrations and flow rates. Such a spread in experimental data is typical of two-phase flow heat transfer experiments as reviewed in Ref. [45] and references therein. Overall, the data appeared to be consistent and overlap relatively well despite the large variation in microfoam morphology, rheological behavior, as well as imposed flow rates and heat fluxes. It is important to note that poor agreement was observed when

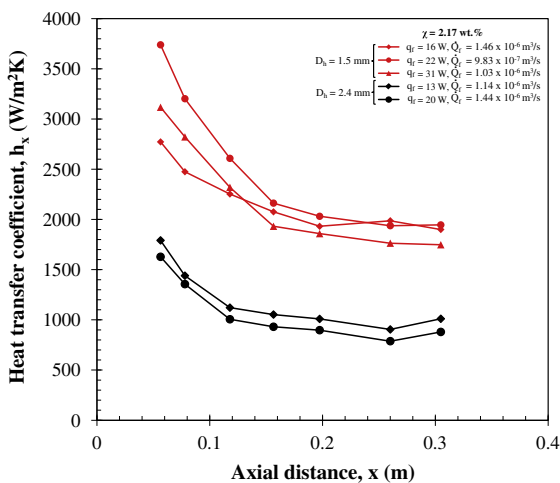


Fig. 3. Local heat transfer coefficient calculated from Eq. (23) versus axial length x for microfoam made from Tween 20 aqueous solution with concentration $\chi = 2.17$ wt.% flowing in 1.5 and 2.4 mm diameter tubes under different heat transfer rates q_f and mass flow rates Q_f .

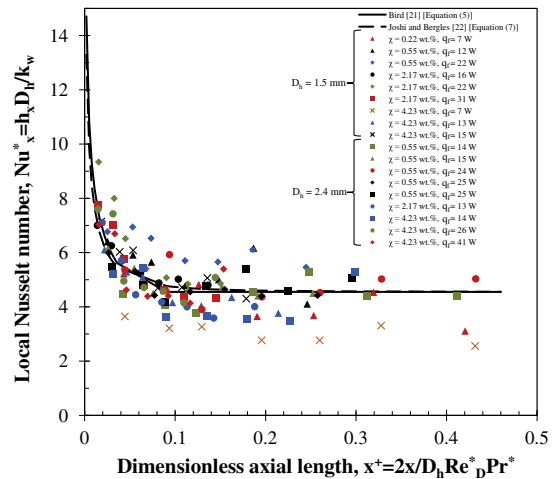


Fig. 4. Comparison between experimental data and model predictions for the local Nusselt number $Nu_x^* = h_x D_h / k_w$ as a function of dimensionless axial length $x^+ = 2x/D_h Re_D^* Pr^*$ for microfoams with different surfactant mass fractions flowing in uniformly heated pipes. The dimensionless numbers were defined in Eq. (24) while the models derived by Bird [21] and Joshi and Bergles [22] were given by Eqs. (5) and (7), respectively.

defining Nu_x^* and Pr^* using the effective thermal properties c_p and k of the microfoam given by previously mentioned EMAs. This indicates that the expression of the dimensionless numbers Nu_x^* , Re_D^* , and Pr^* given by Eq. (24) properly captured the phenomena taking place in convective heat transfer in microfoams flowing in uniformly heated pipes.

Moreover, Fig. 4 also plots the analytical expressions of Nu_x^* for power-law fluids given by Eqs. (5) and (7) proposed by Bird [21] and Joshi and Bergles [22], respectively. Here, the index n was taken as 2/3. Given the experimental uncertainty, the experimental data for the Nusselt number are in good agreement with the model predictions for all microfoams and test conditions investigated. In fact, the average deviation between the fully developed Nusselt number $Nu_{\infty}^* = 4.55$ or 4.56 predicted by Eqs. (5) and (7), respectively and the experimental values of Nu_{∞}^* was less than 18%.

Finally, we speculate that the same results will be valid for microfoams made with other surfactants (e.g., CTAB, SDS) by analogy with previous isothermal rheological studies [16,20]. However, it is unclear if the same approach would prevail for laminar forced convection under constant wall temperature, for turbulent convective heat transfer, and forced convection in different geometries such as rectangular channels and tube bundles. If so, existing correlations for single-phase pseudoplastic fluids could be easily extended to two-phase pseudoplastic fluids such as foams by defining the dimensionless numbers according to Eq. (24) and using the non-Newtonian correction factor introduced by Mizushima et al. [23], and successfully used by Joshi and Bergles [22], to account for the non-Newtonian behavior of microfoams. The next two sections aims to demonstrate the validity and generality of this approach.

4.4. Convective heat transfer to microfoams in rectangular minichannels

In order to apply the correlation giving $Nu_{x,3}^*$ for single-phase Newtonian fluid flowing in laminar flow in rectangular pipes heated from 3 walls to the data reported by Tseng et al. [26], Eqs. (9) and (10) were modified with the non-Newtonian correction factor $[(3n + 1)/4n]^{1/3}$ so that

$$Nu_{x,3}^* = \frac{h_x D_h}{k} = Nu_{x,4} \left(\frac{Nu_{\infty,3}^*}{Nu_{\infty,4}^*} \right) \left(\frac{3n + 1}{4n} \right)^{1/3} \quad (25)$$

and

$$Nu_{\infty,i}^* = Nu_{\infty,i} \left(\frac{3n+1}{4n} \right)^{1/3} \quad \text{with } i = 3 \text{ or } 4 \quad (26)$$

where $Nu_{x,3}$ and $Nu_{\infty,3}$ are given by Eqs. (9) and (10) for Newtonian fluids while $Nu_{x,3}^*$ and $Nu_{\infty,3}^*$ are their counterparts for pseudoplastic fluids. Note that $Nu_{\infty,3}^*/Nu_{\infty,4}^* = Nu_{\infty,3}/Nu_{\infty,4}$.

Fig. 5 shows the local Nusselt number $Nu_{x,3}^*$ versus the dimensionless axial length $x^+/2 = x/D_h Re_D^* Pr^*$ obtained with microfoams flowing in rectangular minichannels ($\alpha = 2.08$) heated from three sides under various heat fluxes and flow rates as reported by Tseng et al. [26]. Here also, the dimensionless numbers $Nu_{x,3}^*$, Re_D^* , and Pr^* for microfoams were defined according to Eq. (24). Fig. 5 indicates that $Nu_{x,3}^*$ decreased in the entry region and rapidly reached a constant value in the fully developed region. Furthermore, it is evident that the experimental data overlap quite well in the fully developed region thus further confirming that the expressions for the dimensionless numbers given by Eq. (24) properly capture the phenomena occurring in convective heat transfer in microfoams under laminar flow conditions. Fig. 5 also plots the modified correlations for convective heat transfer of pseudoplastic fluids under laminar flow in rectangular channels for both the local and fully developed Nusselt number given by Eqs. (25) and (26), respectively. Here also, the flow index n was taken as $2/3$ [16,18–20]. Given the experimental uncertainty and the accuracy of the empirical correlations, the predictions of the modified correlations were in reasonable agreement with experimental data for the broad range of physical conditions considered.

4.5. Convective heat transfer to macrofoams in tube bundles

In this section, the data reported by Gyllys et al. [14,15,46] and previously discussed were used. In these measurements, the cross-sectional area A was equal to 0.02 m^2 while $l_T = l_L = 1.5$ for the aligned tubes and $l_T = 3.5$ and $l_L = 0.875$ for the staggered tubes. Figs. 6a and 7a plots the average heat transfer coefficient versus U_{max} reported for foam flows across aligned and staggered arrangements, respectively [14,15,46]. They indicate that the heat transfer coefficient increases with increasing flow velocities. Note that the measured heat transfer coefficients were independent of tube location for tubes A4, B4, and C4 in aligned tube bundles and for tubes

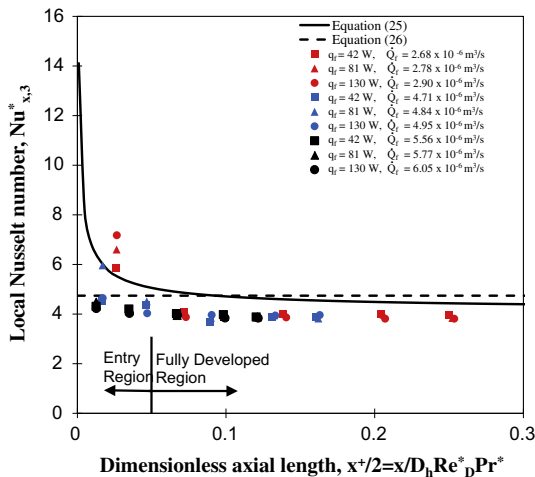


Fig. 5. Comparison between experimental data and model predictions for the local Nusselt number $Nu_{x,3}^* = h_x D_h / k_w$ as a function of dimensionless axial length $x^+/2$ for aqueous microfoams made with Tween 20 and flowing through a rectangular minichannel heat from three surfaces under different imposed heat fluxes and flow rates [26]. The dimensionless numbers were defined in Eq. (24) while the models modified to account for non-Newtonian fluids were given by Eqs. (25) and (26).

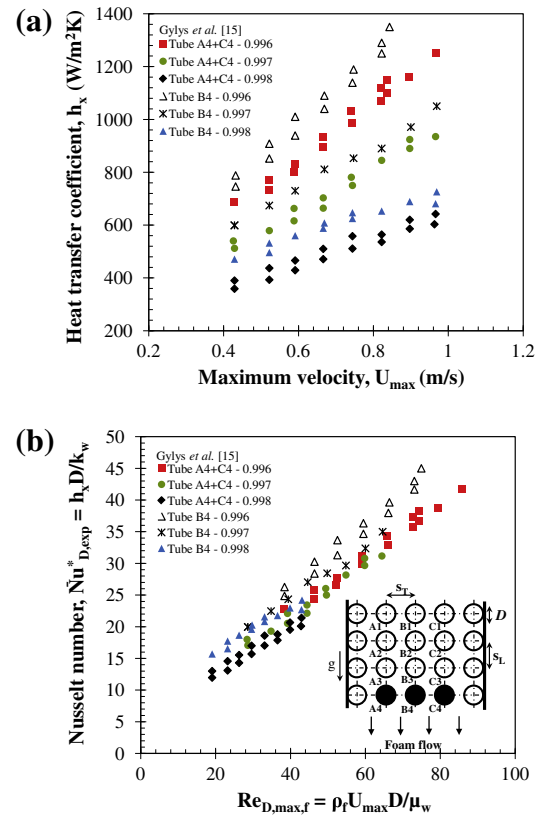


Fig. 6. (a) Average heat transfer coefficient as a function of maximum velocity U_{max} measured by Gyllys et al. [15] and (b) average experimental Nusselt number defined in Eq. (27) versus $Re_{D,max,f} = \rho_f U_{max} D / \mu_w$ for downward flowing foams across tubes A4, B4, and C4 in aligned tube bundles.

A3 and C3 in staggered tubes. Then, at these locations the flow was thermally fully developed.

Moreover, by analogy with the previous analysis for convective heat transfer in microfoams, the experimental average Nusselt number was defined based on the thermal conductivity of water in contact with the tubes as [32]

$$\overline{Nu}_{D,exp}^* = \frac{hD}{k_w} \quad (27)$$

Similarly, the Reynolds and Prandtl numbers for macrofoams in tube bundles were defined as

$$Re_{D,max,f}^* = \frac{\rho_f U_{max} D}{\mu_f} \quad \text{and} \quad Pr^* = \frac{c_{p,w} \mu_f}{k_w} \quad (28)$$

where ρ_f and μ_f are the foam density and viscosity while k_w and $c_{p,w}$ are the water thermal conductivity and specific heat, respectively. If the conclusions for microfoams can be applied to convective heat transfer macrofoams, the correlation developed by Khan et al. [32] for Newtonian fluids could be extended to macrofoams and expressed as

$$\overline{Nu}_{D,th}^* = C_5 C(\chi)^{-1/6} (Ca^*)^{1/18} \left(\frac{\rho_f U_{max} D}{\mu_w} \right)^{1/2} Pr_w^{1/3} \left(\frac{3n+1}{4n} \right)^{1/3} \quad (29)$$

where Pr_w is the Prandtl number of water while the term $[(3n+1)/4n]^{1/3}$ is the non-Newtonian correction factor introduced by Mizushima et al. [23]. The effective foam viscosity μ_f given by Eq. (4) as well as $C(\chi)$ and Ca^* could not be estimated from the data provided by Gyllys et al. [14,15]. However, the terms $C(\chi)^{-1/6}$ and $(3n+1)/4n$ appearing in the above equation are constant for a given surfactant used to make the foaming solution.

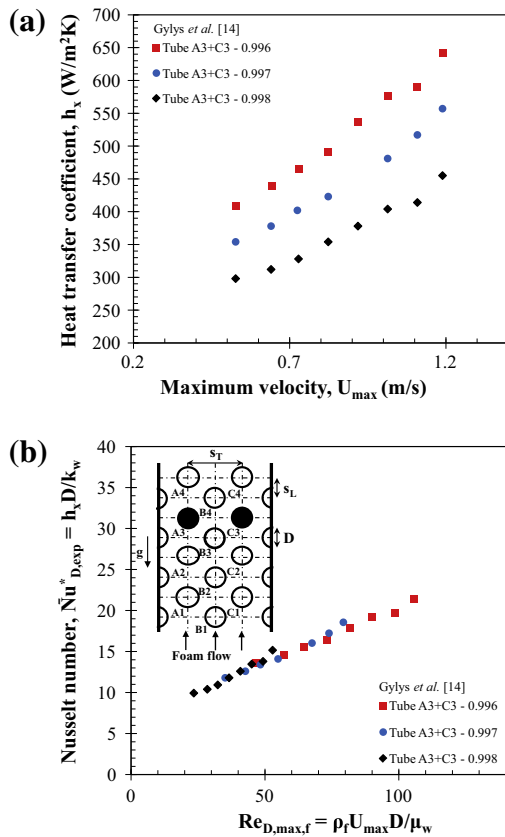


Fig. 7. (a) Average heat transfer coefficient in the fully developed region as a function of maximum velocity U_{max} measured by Gyllys et al. [14] and (b) average experimental Nusselt number defined in Eq. (27) versus $Re_{D,max,f}^* = \rho_f U_{max} D / \mu_w$ for upward flowing foams across tubes A3 and C3 in staggered tube bundles.

Figs. 6b and 7b plot the experimental average Nusselt number $\overline{Nu}_{D,exp}$ given by Eq. (27) versus $\rho_f U_{max} D / \mu_w$ for the same locations in the aligned and staggered tube bundle arrangements as those shown in Figs. 6a and 7a. It is evident that the data collapse on a single line indicating the dimensionless numbers $\overline{Nu}_{D,exp}$ and $Re_{D,max,f}^*$ capture the physical phenomena occurring in the macro-foam flow across the tube bundles. The slight spread in the data can be attributed to variations in foam porosity, bubble size distribution, rheological behavior, as well as in imposed flow rates and temperature. Finally, in order to fully validate Eq. (29), and in particular the non-Newtonian correction factor and the term $C(\chi)^{-1/6}(Ca^*)^{1/18}$, experiments with foams made from solutions with different surfactants and/or fluids other than water should be performed. Their bubble radius, surface tension, and effective viscosity should also be known or measured.

5. Conclusion

The present study collected and analyzed experimental data for convective heat transfer of microfoams in laminar flow condition in circular tubes under constant wall heat flux. Microfoams were made from aqueous solutions with Tween 20 surfactant concentrations with mass fraction ranging from 0.22 to 4.23 wt.%. A wide range of porosity, viscosity, flow rate, heat flux, and two different pipe diameters were explored. The results were compared with existing analytical and semi-empirical dimensionless correlations developed and validated with single-phase power-law fluids. Here, the Reynolds number Re_D^* was defined using the effective density and viscosity of microfoams. However, the dimensionless numbers

Nu_x^* and Pr were defined based on the thermal properties of water. This can be justified by the fact that the heated pipe wall was in direct and continuous contact with a thin layer of water which controlled convective heat transfer to the foam. Good agreement was observed between the model predictions and experimental data when defining Nu_x^* , Re_D^* , and Pr^* according to Eq. (24). The same approach was successfully applied to experimental data collected for laminar flow of microfoams in rectangular minichannels heated from three walls and macrofoams across aligned and staggered tube bundles [14,15]. Finally, it remains to be determined whether this simple and convenient approach can be extended to convective heat transfer in foams made of different fluids under different geometries and/or flow and boundary conditions.

Acknowledgements

The authors would like to thank Professor Vijay Dhir and Dr. Gopinath Warriar for providing equipment and for useful technical discussions.

References

- [1] F. Sebba, Foams and Biliquid Foams-Aphrons, John Wiley & Sons, New York, NY, 1987.
- [2] P. Jauregi, G.R. Mitchell, J. Varley, Colloidal gas aphrons (CGA): dispersion and structural features, *AIChE Journal* 46 (1) (2000) 24–36.
- [3] G. Spigno, P. Jauregi, Recovery of gallic acid with colloidal gas aphrons (CGA), *Int. J. Food Eng.* 1 (4) (2005). Article 5.
- [4] P. Jauregi, J. Varley, Colloidal gas aphrons: a novel approach to protein recovery, *Biotechnol. Bioeng.* 59 (1998) 471–481.
- [5] M.A. Hashim, S. Mukhopadhyay, B.S. Gupta, J.N. Sahu, Application of colloidal gas aphrons for pollution remediation, *J. Chem. Technol. Biotechnol.* 87 (3) (2012) 305–324.
- [6] D. Roy, K.T. Valsarag, W.D. Constant, M. Darji, Removal of hazardous oily waste from a soil matrix using surfactants and colloidal gas aphron suspensions under different flow conditions, *J. Hazardous Mater.* 38 (1994) 127–144.
- [7] D. Roy, R.R. Kommalapti, K.T. Valsarag, W.D. Constant, Soil flushing of residual transmission fluid: application of colloidal gas aphron suspensions and conventional surfactant solutions, *Water Res.* 29 (1995) 589–595.
- [8] R.W. Grimes, Evaluation of a method using colloidal gas aphrons to remediate metals contaminated mine drainage waters, Western Research Institute Report WRI-02-R007, 2002.
- [9] S. Ciriello, S.M. Barnett, F.J. Deluise, Removal of heavy-metals from aqueous-solutions using microgas dispersions, *Separat. Sci. Technol.* 4 (1982) 521–534.
- [10] J. Weber, F.A. Agblevor, Microbubble fermentation of *trichoderma reesei* for cellulase production, *Process Biochem.* 40 (2) (2005) 669–676.
- [11] M.D. Bredwell, R.M. Worden, Mass transfer properties of microbubbles. 1. Experimental studies, *Biotechnol. Progress* 14 (1998) 31–38.
- [12] N.S. Deshpande, M. Barigou, The flow of gas-liquid foams through pipe fittings, *Int. J. Heat Fluid Flow* 22 (2001) 94–101.
- [13] X. Sun, S. Wang, Y. Bai, S. Liang, Rheology and convective heat transfer properties of borate cross-linked nitrogen foam fracturing fluid, *Heat Transfer Eng.* 32 (1) (2010) 69–79.
- [14] J. Gyllys, S. Sinkunas, T. Zdankus, Analysis of staggered tube bundle heat transfer to vertical foam flow, *Int. J. Heat Mass Transfer* 51 (1–2) (2008) 253–262.
- [15] J. Gyllys, T. Zdankus, R. Jonynas, R. Maladauskas, Experimental investigation of in-line tube bundle heat transfer process to vertical downward foam flow, *Int. J. Heat Mass Transfer* 54 (11–12) (2011) 2326–2333.
- [16] S. Larmignat, D. Vanderpool, H.K. Lai, L. Pilon, Rheology of colloidal gas aphrons (microfoams), *Colloids Surface A: Physicochem. Eng. Aspects* 322 (2008) 199–210.
- [17] F.A. Morrison, *Understanding Rheology*, Oxford University Press, Oxford, UK, 2001.
- [18] N.D. Denkov, V. Subramanian, D. Gurovich, A. Lips, Wall slip and viscous dissipation in sheared foams: effect of surface mobility, *Colloids Surface A: Physicochem. Eng. Aspects* 263 (2005) 129–145.
- [19] N.D. Denkov, S. Tcholakova, K. Golemanov, V. Subramanian, A. Lips, Foam wall friction: effect of air volume fraction for tangentially immobile bubble surface, *Colloids Surface A: Physicochem. Eng. Aspects* 282–283 (2006) 329–347.
- [20] J. Zhao, S. Pillai, L. Pilon, Rheology of colloidal gas aphrons (microfoams) made from different surfactants, *Colloids Surface A: Physicochem. Eng. Aspects* 348 (1–3) (2009) 93–99.
- [21] R.B. Bird, On the theory of heat transfer of non-Newtonian fluid in laminar pipe flow, *Chemie Ingenieur Technik* 31 (9) (1959) 569–572.
- [22] S.D. Joshi, A.E. Bergles, Experimental study of laminar heat transfer to in-tube flow of non-Newtonian fluids, *ASME J. Heat Transfer* 102 (3) (1980) 397–401.

- [23] T. Mizushima, R. Ito, Y. Kuriwake, K. Yahikazawa, Boundary layer heat transfer in a circular tube to Newtonian and non-Newtonian fluids, *Kagaku Kogaku* 32 (1967) 250–255.
- [24] S.W. Churchill, R. Usagi, Dissolution of polydisperse silica grains in glass melts – analysis, *Am. Instit. Chem. Eng. J.* 27 (5) (1972) 1121–1128.
- [25] P. Wibulswas, Laminar Flow Heat Transfer in Noncircular Ducts, Ph.D. Thesis, London University, London, UK, 1966.
- [26] H. Tseng, L. Pilon, G.R. Warrier, Rheology and convective heat transfer of colloidal gas aphrons in horizontal mini-channels, *Int. J. Heat Fluid Flow* 27 (2006) 298–310.
- [27] F.P. Incropera, D.P. DeWitt, *Fundamentals of Heat and Mass Transfer*, fourth ed., John Wiley & Sons, New York, NY, 1996.
- [28] P.S. Lee, S.V. Garimella, Thermally developing flow and heat transfer in rectangular microchannels of different aspect ratios, *Int. J. Heat Mass Transfer* 49 (2006) 3060–3067.
- [29] R.J. Phillips, Microchannel Heat Sinks, Master's Thesis, Massachusetts Institute of Technology, Cambridge, MA, USA, 1987.
- [30] R.K. Shah, A.L. London, *Laminar Flow Forced Convection in Ducts*, Academic Press, New York, NY, 1978.
- [31] W.A. Khan, J.R. Culham, M.M. Yovanovich, Fluid flow around and heat transfer from an infinite circular cylinder, *ASME J. Heat Transfer* 127 (2005) 785–790.
- [32] W.A. Khan, J.R. Culham, M.M. Yovanovich, Convection heat transfer from tube banks in crossflow: analytical approach, *Int. J. Heat Mass Transfer* 49 (2006) 4831–4838.
- [33] W.M. Kays, M.E. Crawford, B. Weigand, *Convective Heat and Mass Transfer*, fourth ed., McGraw-Hill, New York, NY, 2005.
- [34] S. Kakac, Y. Yener, *Convective Heat Transfer*, second ed., CRC Press, Boca Raton, FL, 1995.
- [35] Design Institute for Physical Properties, Thermophysical Properties Database DIPPR 801, <<http://www.aiche.org/dippr/products/801.aspx>>, 2012.
- [36] G.C.J. Bart, Thermal Conduction in Non Homogeneous and Phase Change Media, Ph.D. Thesis, Delft University of Technology, 1987.
- [37] H.W. Russell, Principles of heat flow in porous insulators, *J. Am. Ceramic Soc.* 18 (1935) 1–5.
- [38] G.S. von Frey, Über die elektrische Leitfähigkeit binärer Aggregate, *Z. Elektrochem. Angew. Phys. Chem.* 38 (5) (1932) 260–274.
- [39] Lord Rayleigh, On the influence of obstacles arranged in rectangular order upon the properties of a medium, *Philos. Mag.* 34 (1892) 481–502.
- [40] D.A. De Vries, The Thermal Conductivity of Granular Materials, Annex 1952-1 Bulletin of the International Institute of Refrigeration, 1952, pp. 115–131.
- [41] J.C. Maxwell, *A Treatise on Electricity and Magnetism*, vol. 1, third ed., Oxford University, New York, NY, 1892.
- [42] D.A.G. Bruggeman, Berechnung verschiedener physikalischer konstanten von heterogenen substanzen, *Ann. Phys.* 24 (2) (1935) 636–679.
- [43] B. Alazmi, K. Vafai, Analysis of variants within the porous media transport models, *Int. J. Numer. Methods Fluids* 122 (2) (2000) 303–326.
- [44] J. L ev eque, Les lois de la transmission de la chaleur par convection, *Ann. Mines* 13 (1926), pp. 201, 305, 381.
- [45] A.J. Ghajar, C.C. Tang, Importance of non-boiling two-phase flow heat transfer in pipes for industrial applications, *Heat Transfer Eng.* 31 (9) (2010) 711–732.
- [46] J. Gylys, T. Zdankus, I. Gabrielaitiene, S. Sinkunas, Experimental research of heat transfer from an in-line tube bundle to a vertical foam flow, *Heat Transfer Res.* 40 (5) (2009) 455–472.